Analyst

Accepted Manuscript

ROYAL SOCIETY OF CHEMISTRY

www.rsc.org/analyst

Analyst

Revised; 29 November 2014

Tandem mass spectrometry and ion mobility mass spectrometry for the analysis of molecular sequence and architecture of hyperbranched glycopolymers

Xiumin Liu,[a] Lydia R. Cool,[a] Kenneth Lin,[b] Andrea M. Kasko[b] and Chrys Wesdemiotis*,[a]

[a] Department of Chemistry, The University of Akron, Akron, OH 44325-3601, USA. E-mail: wesdemiotis@uakron.edu; Fax: +1-330-972-6085; Tel.: +1-330-972-7699.

[b] Department of Bioengineering, University of California, Los Angeles, CA 90095, USA.

† Electronic supplementary information (ESI) available.

Abstract

Multidimensional mass spectrometry techniques, combining matrix-assisted laser desorption/ionization (MALDI) or electrospray ionization (ESI) with tandem mass spectrometry (MS^2), multistage mass spectrometry (MS^n) or ion mobility mass spectrometry (IM-MS), have been employed to gain precise structural insight on the compositions, sequences and architectures of small oligomers of a hyperbranched glycopolymer, prepared by atom transfer radical copolymerization of an acrylate monomer (A) and an acrylate inimer (B), both carrying mannose ester pendants. The MS data confirmed the incorporation of multiple inimer repeat units, which ultimately lead to the hyperbranched material. The various possible structures of *n*-mers with the same composition were subsequently elucidated based on MS^2 and MS^n studies. The characteristic elimination of bromomethane molecule provided definitive information about the comonomer connectivity in the copolymeric AB_2 trimer and A_2B_2 tetramer, identifying as present only one of the three possible trimeric isomers (*viz.* sequence BBA) and only two of the six possible tetrameric isomers (*viz.* sequences BBA_2 and BABA). Complementary IM-MS studies confirmed that only one of the tetrameric structures is formed. Comparison of the experimentally determined collision cross-section of the detected isomer with those predicted by molecular simulations for the two possible sequences ascertained BBA_2 as the predominant tetrameric architecture. The multidimensional MS approaches presented provide connectivity information at the atomic level without requiring high product purity (due to the dispersive nature of MS) and, hence, should be particularly useful for the microstructure characterization of novel glycopolymers and other types of complex copolymers.

Introduction

Carbohydrates participate in numerous biological functions in living systems, which are generally initiated by molecular recognition events proceeding through specific, noncovalent carbohydrate-protein interactions.[1-5] Saccharides that bind weakly to protein receptors may not provide sufficient control for processes mediated *in vivo* by protein-carbohydrate binding. This problem has spurred the development of synthetic carbohydrates and carbohydrate-based polymers ("glycopolymers") that interact more strongly with proteins due to their multiple sugar residues.[3,4] Interest in such polymers has further increased after several studies revealed that glycopolymer-protein interactions are very similar with those between proteins and natural (poly)saccharides and suitable for a diverse array of pharmaceutical and medical applications, including drug delivery, diagnosis, immune system modulation and tissue engineering.[3,6-11] Glycopolymers are also employed as superabsorbents, contact lens materials and gene delivery systems due to their biocompatibility and biodegradability.[12-16] The term "glycopolymer" describes both synthetic carbohydrates as well as carbohydrate-bearing polymers in which sugar moieties are attached as pendants to a conventional synthetic polymer chain.[8]

The chemical properties of a glycopolymer and its suitability for a specific biomedical application depend on the spatial arrangement of its sugar units.[4] Preparing and identifying specific structures is therefore essential for glycopolymers intended for medical use. Glycopolymers can exist in different architectures, including branched, dendritic and comb-shaped structures.[8] As with natural carbohydrates,[17] isomeric sequences of the individual repeat units are possible, posing significant challenges in deducing the correct connectivity (primary structure) and overall shape of a glycopolymer.

The progress achieved in glycotechnology over the last decades has been accompanied by a comparable development of analytical methods for the characterization of natural and synthetic carbohydrates. Among them, mass spectrometry (MS) has become an established and widely used technique for the analysis of carbohydrates, providing molecular structure information with high sensitivity and convenient sample preparation.[17-24] In particular, tandem mass spectrometry (MS^2) and multistage mass spectrometry (MS^n) *via* collisionally activated dissociation (CAD) have proven to be a powerful means for the determination of the primary structure of carbohydrates.[20,22-25] These methods have found similar practicality in analyses of synthetic polymer connectivity.[26-39] More recently, ion mobility mass spectrometry (IM-MS)[40-43] has shown promise in offering unique insight into both carbohydrate branching and stereochemistry[22,44,45] as well as into synthetic polymer assembly and architecture.[39,46-55] The present investigation evaluates for the first time the utility of combining MS^2, MS^n and IM-MS to determine the sequence (primary structure) and architecture (branching type) of a glycopolymer. The sample examined was a copolymer synthesized from an acrylate monomer (A) and an acrylate inimer (B), both containing a β-D-mannopyranoside substituent in the ester moiety (Fig. 1);[56] these units can copolymerize to yield linear chains with all mannose groups as pendants or branched chains with some mannose groups as pendants and some within the chain at the branching points, as shown in Fig. 1.

Experimental

Materials

The glycopolymer studied was prepared *via* atom-transfer radical polymerization (ATRP) of a 2:1 molar mixture of acetyl protected acryloyl-β-D-mannopyranoside (structure A in Fig. 1) and

acetyl protected acryloyl-1-(2-bromo)-methyl acrylic-β-D-mannopyranoside (structure B in Fig. 1), as has been reported in the literature.[56] Gel permeation chromatography (GPC) analysis, using poly(methyl methacrylate) standards for mass scale calibration, indicated an average molecular weight (M_n) of 6080 Da and a polydispersity index (M_w/M_n) of 1.86.[56]

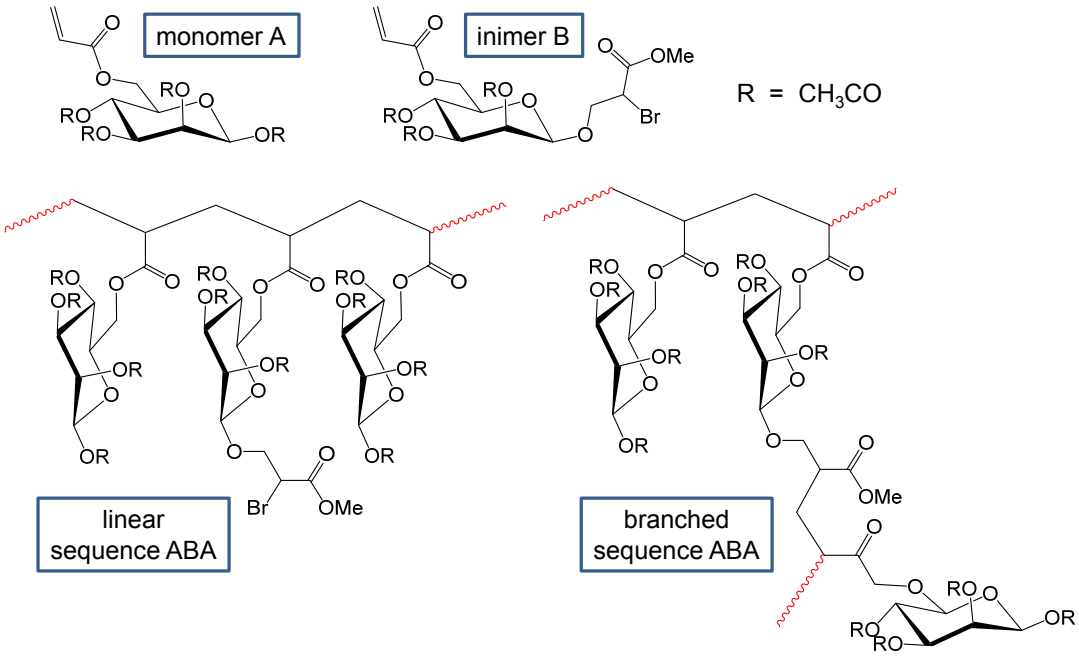

Fig. 1. Monomer and inimer used for the synthesis of the glycopolymer studied (top); the inimer includes both an initiating moiety and a polymerizable group. The monomer and inimer can copolymerize to yield linear and branched chain segments (bottom).

Matrix-assisted laser desorption/ionization (MALDI) experiments

MALDI-MS and MS^2 experiments were carried out on a Bruker UltraFlex III tandem time-of-flight (ToF/ToF) mass spectrometer (Bruker Daltonics, Billerica, MA), equipped with a Nd:YAG laser emitting at a wavelength of 355 nm; t-2-[3-(4-t-butyl-phenyl)-2-methyl-2-propenylidene]malononitrile (DCTB) was used as matrix and sodium trifluoroacetate (NaTFA)

as cationizing agent. Solutions of the matrix (20 mg/mL), polymer (20 mg/mL) and cationizing salt (10 mg/mL) were prepared in $CHCl_3$ and mixed in the ratio 10:5:1, respectively. Approximately 0.5 μL of the final mixture was spotted on a 384-well ground-steel MALDI plate and allowed to air-dry before insertion of the plate into the vacuum system. MS^2 experiments were performed using Bruker's LIFT mode with no additional collision gas.[57] Data analysis was conducted with the flexAnalysis software.

Electrospray ionization (ESI) experiments

Stock solutions of the polymer and NaTFA were prepared in $CHCl_3$ and MeOH, respectively (both at 10 mg/mL). The samples sprayed were prepared by mixing 10 μL of the polymer solution with 1 μL of the salt solution and adding 750 μL $CHCl_3$ and 250 μL MeOH to obtain a final polymer concentration of 0.10 mg/mL in 3:1 (v/v) $CHCl_3$/MeOH.

MS^n. The final polymer solution was injected into a Bruker HCTultra II quadrupole ion trap (QIT) mass spectrometer (Bruker Daltonics, Billerica, MA)[58] by direct infusion with a syringe pump at a flow rate of 180 μL/h. The temperature and flow rate of the drying gas (N_2) were 300 ºC and 8 L/min, respectively; the pressure of the nebulizing gas (N_2) was set at 10 psi. MS^2 spectra were acquired by isolating the appropriate precursor ion and accelerating it with an RF field in order to induce collisionally activated dissociation (CAD) with the He bath gas in the QIT; for MS^n spectra (n = 3-4), the isolation and activation procedure were repeated with a specific fragment in the MS^2 and MS^3 spectra, respectively.

IM-MS. The glycopolymer architecture was examined by ion mobility mass spectrometry (IM-MS) on a Waters Synapt HDMS quadrupole/time-of-flight (Q/ToF) mass

spectrometer (Waters, Milford, MA), equipped with the traveling wave version of IM-MS.[59] Instrument parameters were adjusted as follows: ESI capillary voltage, 3.5 kV; sample cone voltage, 30 V; extraction cone voltage, 3.2 V; desolvation gas flow, 550 L/h (N_2); trap collision energy (CE), 6.0 eV; transfer CE, 4.0 eV; trap gas flow, 1.5 mL/min (Ar); IM gas flow, 22.7 mL/min (N_2); sample flow rate, 10 μL/min; source temperature, 90 °C; desolvation temperature, 180 °C; IM traveling wave velocity, 350 m/s; and IM traveling wave height, 10.5 V.

Collision cross-section determination

The collision cross-section (CCS) of oligomers with the composition A_2B_2 was deduced from the corresponding drift time, measured by IM-MS, after calibration of the drift time scale with ions of known CCS as reported previously.[60-62] Polyalanine, cytochrome c and insulin chain A ions served as calibrants.[63] The calibration curve was constructed by plotting the corrected CCSs of the calibrant ions against their corrected drift times measured by IM-MS at the same instrument settings used for the glycopolymer (see Electronic Supplementary Information).

Molecular modeling

Geometry optimization of glycopolymer structures with the composition A_2B_2 was performed by molecular mechanics/dynamics calculations, using the Materials Studio software (version 4.2). With each architecture, 150 candidate structures were generated and their theoretical collision cross-sections were calculated by the projection approximation method available in the MOBCAL software program.[64]

RESULTS AND DISCUSSION

MALDI-MS analysis

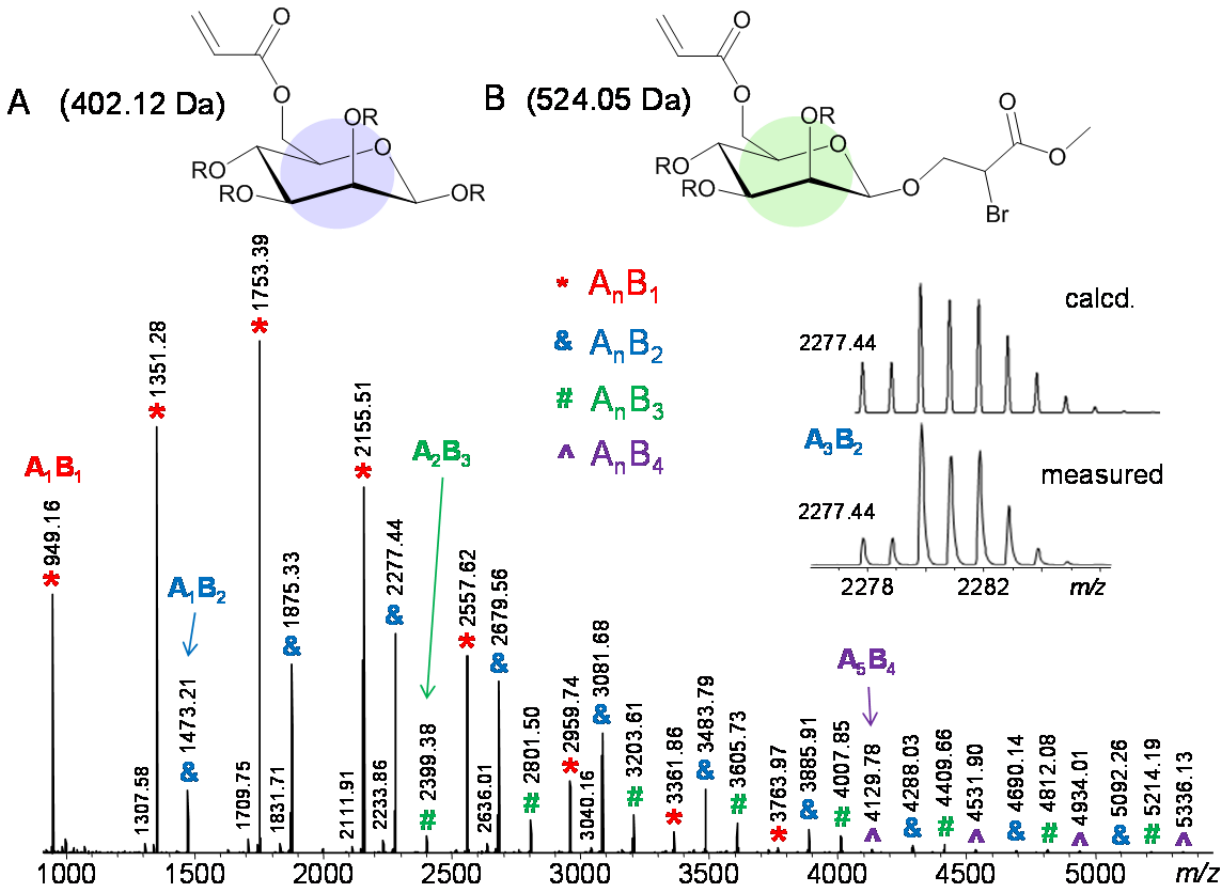

Fig. 2. MALDI mass spectrum of the glycopolymer studied. Four $[M + Na]^+$ ion distributions of A_nB_m oligomers, m = 1-4, are clearly discerned. Each oligomer observed includes m Br atoms. The insets show the structures of A and B (with their pendants shadowed by different colors) and the measured and calculated isotope pattern of one oligomer (A_3B_2), which corroborates the detection of brominated acrylates upon MALDI. Monoisotopic m/z ratios are given on top of the peaks. R = CH_3CO.

The MALDI mass spectrum of the acetyl protected glycopolymer is shown in Fig. 2. It shows four distributions with the composition $[A_nB_m + Na]^+$ (m = 1-4). The mass difference between

two consecutive peaks within each distribution is 402 Da, matching the mass of one A unit (monomer). Because each B unit (inimer) contributes one Br atom, oligomers with the composition A_nB_m should contain *m* Br atoms; this is confirmed by the mass-to-charge ratios and isotope patterns of the corresponding oligomer peaks, as exemplified in Fig. 2 for A_3B_2 (*m/z* 2277.44). Similarly, the other ions detected in the MALDI mass spectrum include all Br atoms provided by their inimer content.

A higher number of inimer units in the glycopolymer lead to higher molecular weight. This is reflected by the average molecular weights (M_n) of the four A_nB_m distributions observed in the MALDI mass spectrum, which increase from 1878 Da for A_nB_1 to 2609 Da for A_nB_2, 3411 Da for A_nB_3 and 4134 Da for A_nB_4. Such a trend is consistent with the formation of simultaneously growing branches after inimer incorporation.

Tandem mass spectrometry analysis

A_nB_1 oligomers. Linear as well as branched architectures are possible for $A_nB_{>1}$. Conversely, the major distribution, A_nB_1, can only have a linear structure with the inimer and its acryloyl group at the initiating chain end and a Br atom at the terminating chain end. The MS^n characteristics of oligomers A_1B_1, A_2B_1 and A_3B_1 were examined first, using QIT multistage mass spectrometry, in order to evaluate the fragmentation pathways of linear chain segments.

Collisionally activated A_1B_1 mainly undergoes consecutive and competitive decompositions *via* 1,5-H rearrangement at either the acetyl protecting groups or the glycopolymer backbone ester groups, giving rise to neutral losses of acetic acid (AcOH, 60 Da) and ketene (CH_2CO, 42 Da), or the fully protected mannose pendant with an exocyclic double

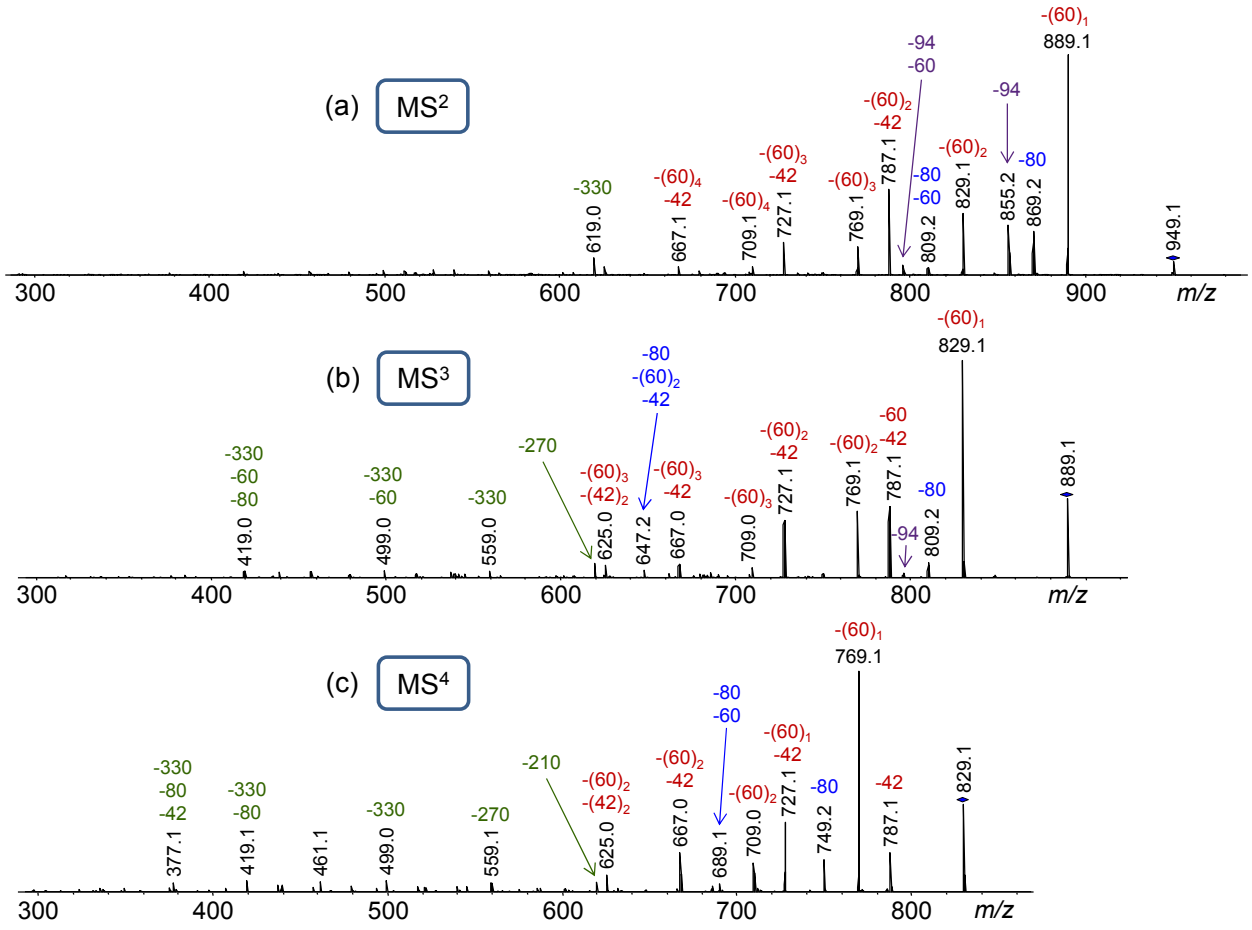

Fig. 3. (a) ESI-MS^2 (CAD) mass spectrum of sodiated A_1B_1 (*m/z* 949.1); (b) MS^3 (CAD) mass spectrum of *m/z* 889.1, formed by acetic acid (AcOH) loss from sodiated A_1B_1; (c) MS^4 (CAD) mass spectrum of *m/z* 829.1, formed by AcOH loss from *m/z* 889.1. The numbers on top of the peaks give the monoisotopic *m/z* ratio (in black) and the mass of the neutral loss(es) in Da (in color); -60 and -42 indicate losses of acetic acid and ketene, respectively; -80 and -94 indicate losses of HBr and CH_3Br, respectively; -330, -270 and -210 indicate losses of a mannose pendant or a mannose pendant that lost one or two AcOH molecules, respectively. The subscripts indicate the number of losses.

bond (330 Da), respectively (*cf.* Fig. 3a and Scheme 1a-b). Up to two AcOH molecules can be eliminated by this mechanism from each mannose unit of A_1B_1, producing a double bond within

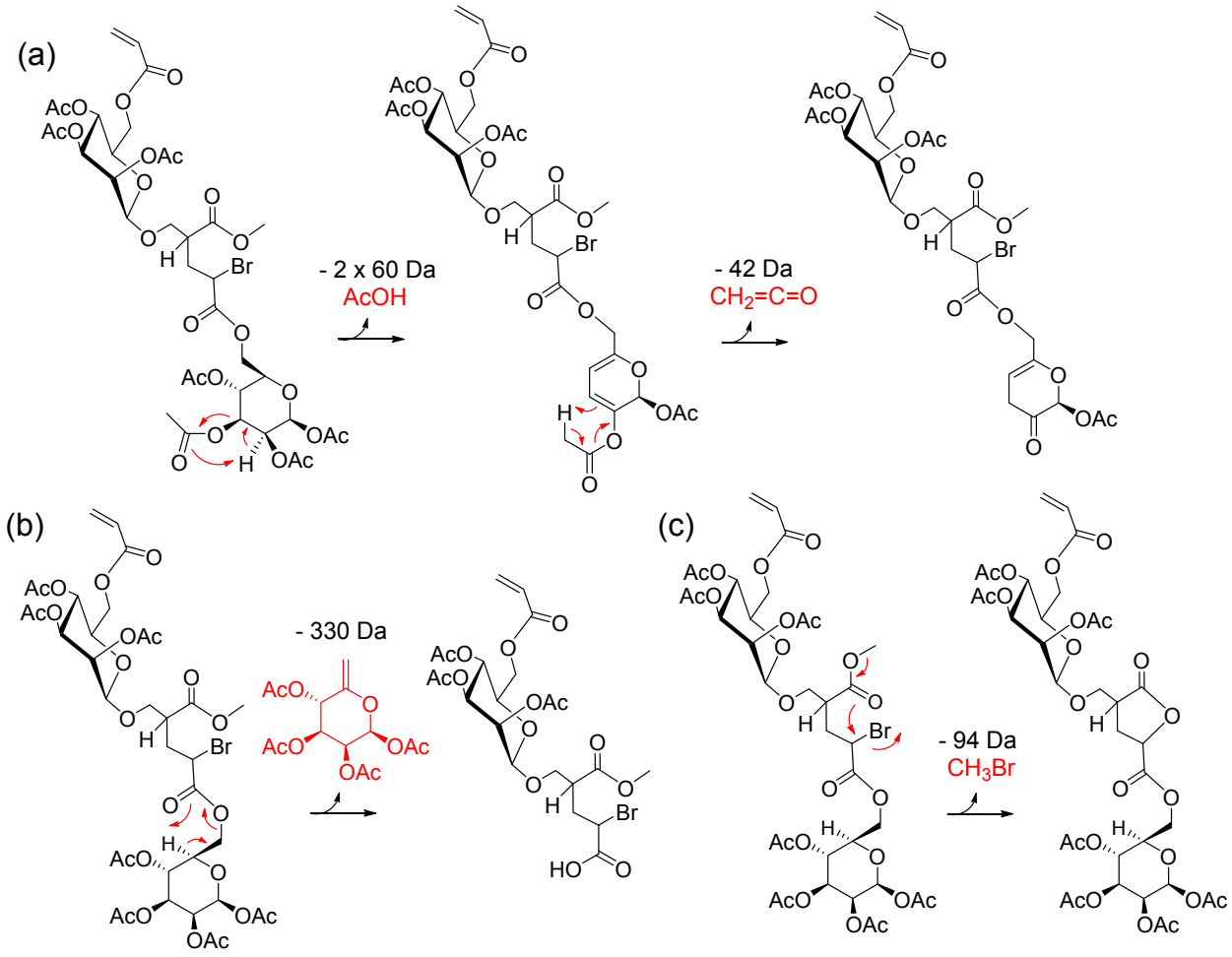

Scheme 1. Charge-remote 1,5-H rearrangements in sodiated A_1B_1, leading to (a) AcOH and CH_2CO losses from the mannose ring and (b) expulsion of the sugar pendant from monomer unit A; the Na^+ has been omitted for brevity. Note that AcOH and CH_2CO losses can occur at the mannose group of A (as shown) as well as the mannose group of B. (c) Intramolecular nucleophilic displacement of Br by the adjacent ester group to form a five-membered ring lactone with concomitant elimination of CH_3Br. The latter reaction is possible only at a terminal unit (A or B) attached at the branching site of an inimer unit B (see text).

the sugar ring after each AcOH loss. After elimination of two AcOH molecules from the same mannose ring, a remaining acetyl group in the same ring can be cleaved in the form of ketene (42 Da) by 1,5-H rearrangement to one of the newly created double bonds, *cf.* Scheme 1. The

successive elimination of two acetic acid and one ketene moieties (*i.e.* the reaction sequence *m/z* 949.1 → 889.1 → 829.1 → 787.1) is supported by the MS^3 and MS^4 characteristics of the CAD fragments generated after the first (*m/z* 889.1) and second AcOH loss (*m/z* 829.1), *cf.* Figs. 3b-3c.

Two additional, major fragmentation pathways of sodiated A_1B_1 are the elimination of HBr (80 Da) and CH_3Br (94 Da), both of which are accompanied by consecutive AcOH losses (Fig. 3a). The loss of HBr (*m/z* 869.2) takes place within the acrylate frame and most likely produces a conjugated double bond. On the other hand, the loss of CH_3Br (*m/z* 855.2) is accounted for by an intramolecular nucleophilic displacement leading to the formation of a favorable, five-membered ring lactone and the expulsion of methyl bromide (*cf.* Scheme 1c).

The fragmentation pathway proposed for the formation of *m/z* 855.2 (Scheme 1c) is supported by the MALDI-MS^2 mass spectrum of A_1B_1 acquired using MALDI-ToF/ToF instrumentation (see Experimental), with which the entire isotope cluster of the precursor ion is mass-selected for MS^2 analysis.[36] In this spectrum (Fig. S1), *m/z* 855.2 does not show the characteristic isotope pattern of Br, confirming that Br is lost with the neutral fragment. Similarly, the presence or absence of Br content in the other MS^2 fragments is readily established from the corresponding isotope patterns (*cf.* Fig. S1).

It is noteworthy that backbone cleavages within the acrylate connectivity are not observed, in analogy to sodiated poly(butyl acrylate)s, which also dissociate mainly by 1,5-H rearrangements at the acrylate pendants and in sharp contrast to sodiated poly(methyl acrylate), which dissociates through homolytic backbone C–C bond cleavages.[65] This reactivity difference must result from the lower energy requirements for dissociations *via* 1,5-H rearrangement

("McLafferty-type" rearrangement) as compared to dissociations proceeding through homolytic bond cleavages in the polymer chain.[35,65]

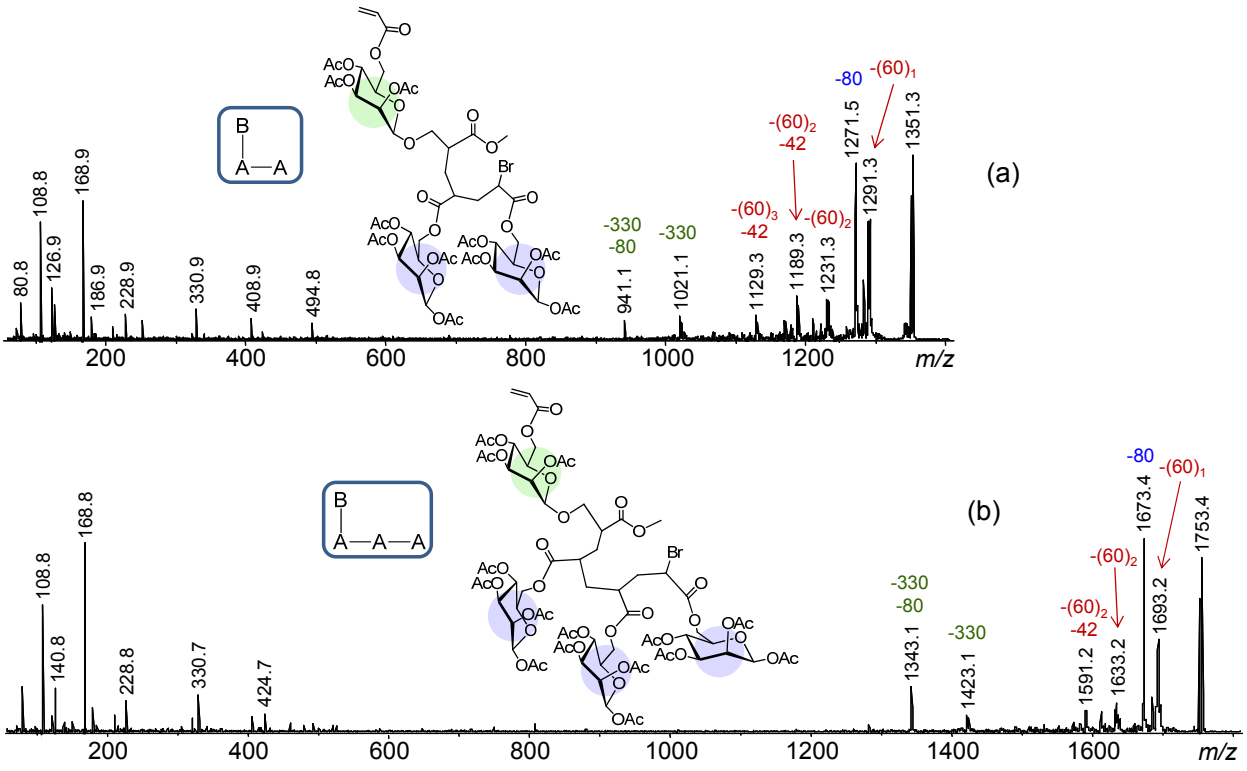

Fig. 4. MALDI-MS^2 mass spectra of sodiated (a) A_2B_1 (*m/z* 1351.3) and (b) A_3B_1 (*m/z* 1753.4); the numbers on top of the peaks give the monoisotopic *m/z* ratio (in black) and the mass of the neutral loss(es) in Da (in color). The insets show the structures of A_2B_1 and A_3B_1.

A_2B_1 and A_3B_1 oligomers. These larger glycopolymer *n*-mers were only examined by MALDI-MS^2 (Fig. 4). The fragmentation pathways of sodiated A_2B_1 and A_3B_1 are fairly similar with those of A_1B_1. Both primarily dissociate by charge remote 1,5-H rearrangements, giving rise to consecutive and competitive losses of 60 Da, 42 Da and 330 Da from the protected sugar pendants, *cf.* Fig. 4. The elimination of hydrogen bromide is also observed from both A_2B_1 and

A_3B_1. The peaks in the low mass range of the MS^2 spectra originate largely from the sugar pendant losses; plausible structures of the most prominent fragments are provided in Fig. S2.

As with A_1B_1, neither A_2B_1 nor A_3B_1 forms any noticeable fragments from cleavages within the polyacrylate backbone. In contrast to A_1B_1, however, the larger *n*-mers do not produce a neutral CH_3Br (94 Da) fragment *via* intramolecular nucleophilic displacement, *cf.* Fig. 4 *vs.* S1. Consequently, the latter reaction can compete with the 1,5-H rearrangements and HBr loss only if the Br atom is in γ position to the propionate carbonyl group of the inimer and CH_3Br elimination leads to the formation of an entropically favored five-membered ring lactone, as is possible for A_1B_1 (*cf.* Scheme 1), but not for $A_{>1}B_1$ where the reacting sites are further apart from each other and hindered by rotational restrictions, due to the presence of bulky sugar pendants, in approaching each other for lactone formation.[66] Observation of CH_3Br loss is, thus, specific to glycopolymer in which a B (inimer) unit is connected through its initiating site to a terminal A or B unit and can be used to probe the sequence and type of branching in smaller oligomers, such as A_1B_2 and A_2B_2 (*vide infra*).

A_1B_2 oligomers. Three isomers with distinct sequences and/or architectures exist for glycopolymer *n*-mers with the composition A_1B_2. These are shown in Fig. 5 in schematic representation using the symbols A and B for the monomer and inimer repeat units, respectively. Horizontal bonds denote repeat unit attachment through the acrylate vinyl group, whereas vertical bonds indicate repeat unit attachment to the initiator site (branching site) of the inimer. All isomers start with a B unit and a vertical bond (because only the inimer can initiate the polymerization), but differ in the sequence and arrangement of the other two repeat units. In the text, monomer or inimer units attached to a vertical bond (*i.e.* repeat units connected to the initiating site of the inimer) are shown in parentheses to avoid ambiguity (*cf.* Fig. 5).

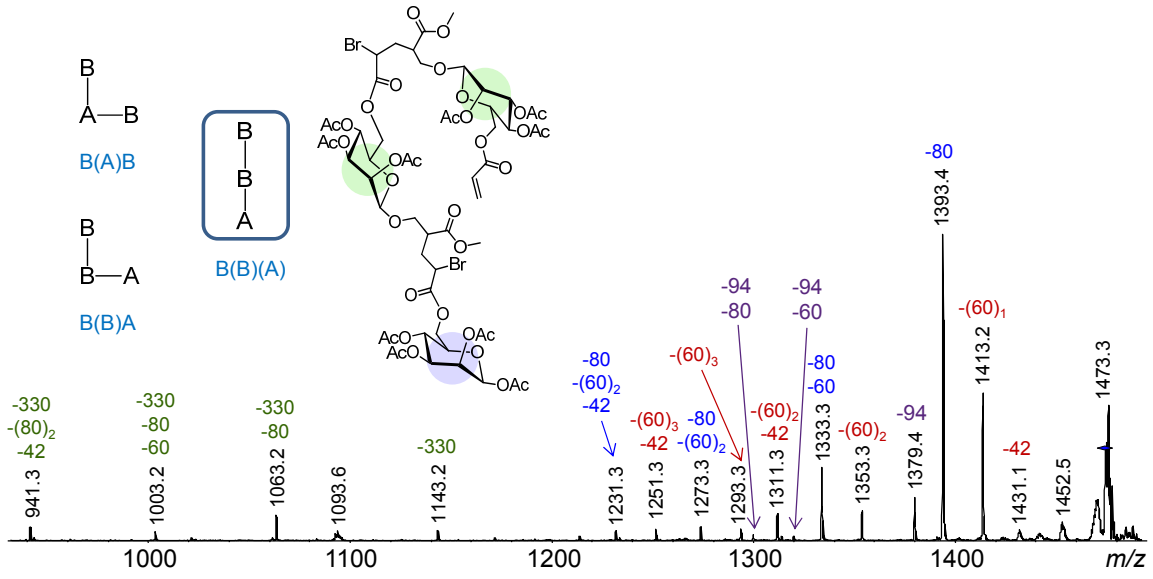

Fig. 5. ESI-MS^2 (CAD) mass spectra of sodiated A_1B_2 (*m/z* 1473.3); the numbers on top of the peaks give the monoisotopic *m/z* ratio (in black) and the mass of the neutral loss(es) in Da (in color). The inset shows schematic representations of the three isomers possible with the A_1B_2 stoichiometry and the actual structure of the A_1B_2 architecture from which CH_3Br can be eliminated to form a five-membered ring lactone.

The ESI-MS^2 mass spectrum of sodiated A_1B_2 (Fig. 5) includes abundant fragments from competitive and sequential eliminations of hydrogen bromide (80 Da), acetic acid (60 Da), ketene (42 Da) and unbranched sugar pendant (330 Da), as observed for the other *n*-mer stoichiometries (Fig. 4) and which affirm the glycopolymer composition but do not provide connectivity information. The loss of methyl bromide (94 Da) and consecutive losses of methyl bromide and acetic acid or hydrogen bromide are, however, also observed, indicating that the major product with A_1B_2 stoichiometry must contain a terminal unit attached to the branching point of the inimer B (*i.e.* a terminal unit connected vertically to a penultimate B). Only one of the three possible A_1B_2 structures, *viz.* B(B)(A), satisfies this requirement and is, thus, identified as the main A_1B_2 product.

A_2B_2 oligomers. The number of distinct isomers for the glycopolymer composition A_2B_2 increases to six. These are shown in Fig. 6a in schematic representation using the symbols A and B and vertical bonds or parentheses to designate chain extension through the inimer branching point (*vide supra*).

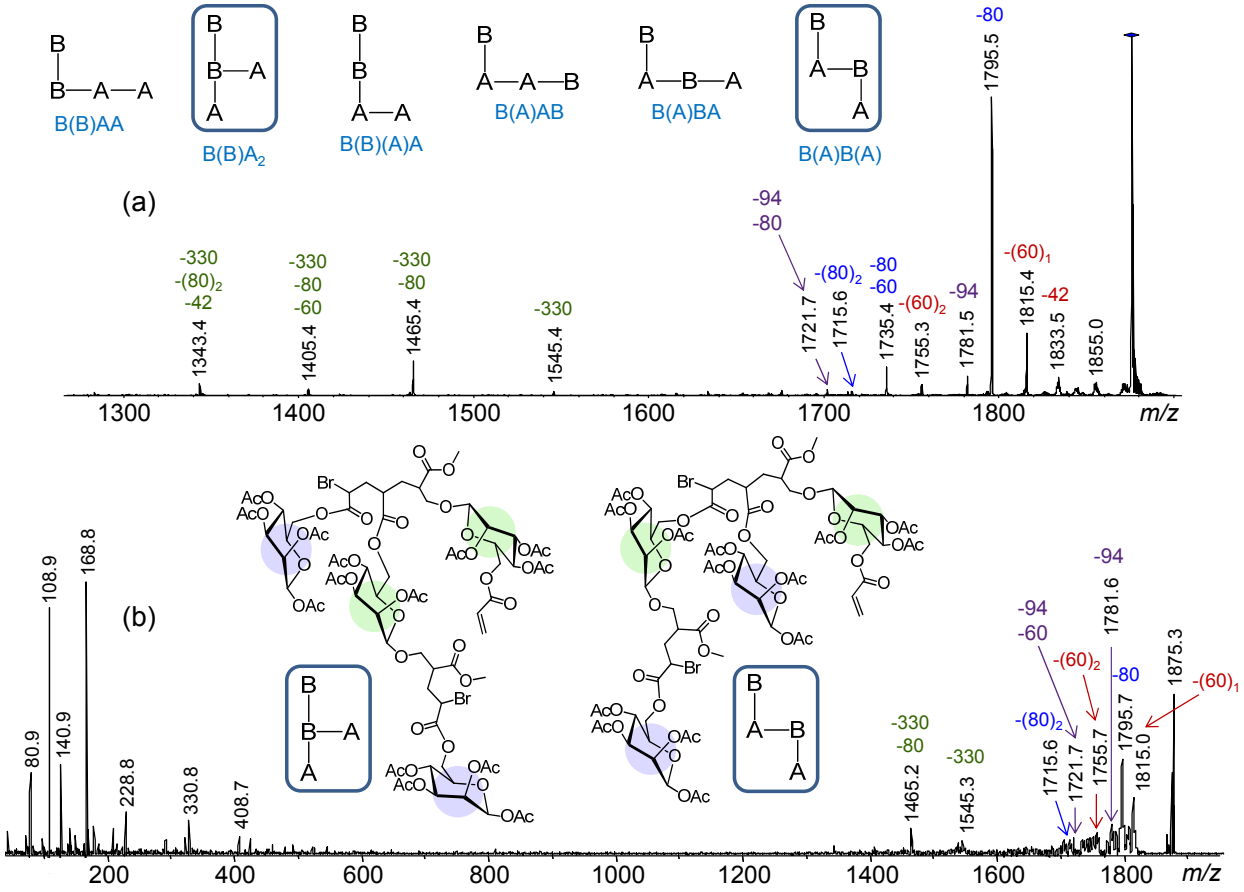

Fig. 6. (a) ESI-MS^2 and (b) MALDI-MS^2 mass spectra of sodiated A_2B_2 (*m/z* 1875.3); the numbers on top of the peaks give the monoisotopic *m/z* ratio (in black) and the mass of the neutral loss(es) in Da (in color). The insets show (a) the isomers possible with the A_2B_2 stoichiometry and (b) the A_2B_2 architectures from which CH_3Br can be eliminated to form a five-membered ring lactone. The low-mass fragments are not detected in the ESI-MS^2 spectrum due to the low-mass cutoff in CAD experiments with QIT instrumentation.[58]

Under both ESI-MS^2 (Fig. 6a) as well as MALDI-MS^2 (Fig. 6b) conditions, sodiated A_2B_2 loses CH_3Br (94 Da) as well as one or more molecules of acetic acid (60 Da), ketene (42 Da) and unbranched sugar pendant (330 Da). The methyl bromide loss again reveals that this *n*-mer must include a terminal unit that is connected to the branching point (initiating site) of an inimer unit. The two sequences shown in Fig. 6b (their schematic acronyms are encased) possess this distinguishing structural feature, which establishes them as the prime A_2B_2 candidates. Confirmatory proof for this conclusion and further differentiation between the two possible architectures was sought by IM-MS (*vide infra*).

The oligomers found to lose CH_3Br, *viz.* dimer BA, trimer B(B)(A) and tetramers B(B)A_2 or B(A)B(A), carry one terminal B(A) unit; consequently, this elimination can only occur at one site. On the other hand, the trimer and tetramers contain two sites where HBr loss can take place, while all four *n*-mers have several acetyl groups from which AcOH loss(es) can proceed. These differences and the rising number of competitive and sequential dissociations that are possible with increasing oligomer size reconcile the decrease in intensity of the CH_3Br loss in the ESI-MS^2 spectra, relative to the total fragment ion current, when the number of comonomer repeat units increases from two (Fig. 3a) to three (Fig. 5) to four (Fig. 6a). Nonetheless, this structurally diagnostic fragment is clearly discernible and appears with an significant intensity in all cases (>6% of most abundant fragment). Interestingly, the peak intensity ratio of CH_3Br loss *versus* the first AcOH loss is fairly constant among the oligomers undergoing both reactions: 0.23 for BA, 0.29 for B(B)(A) and 0.30 for B(B)A_2 / B(A)B(A); this similarity is attributed to the comparable mechanisms of these fragmentations, both of which involve charge-remote rearrangements through cyclic transition states (*cf.* Scheme 1).

Ion mobility mass spectrometry analysis

The $[M + Na]^+$ ions of A_2B_1 (*m/z* 1351) and A_3B_1 (*m/z* 1753), which can only have one architecture (*cf.* Fig. 4), were investigated first. Separation of their constituents by their ion mobilities gave rise to the IM-MS drift time distributions depicted in Figs. 7a-b, which show the presence of three components in each ion beam, arising from superimposed charge states of different oligomers (*cf.* Fig. 7). The isotope patterns of the signals at 7.04, 4.15 and 3.25 ms in Fig. 7a reveal the compositions $[A_2B_1 + Na]^+$, $[A_4B_2 + 2Na]^{2+}$ and $[A_6B_3 + 3Na]^{3+}$, respectively; similarly, the three signals at 10.47, 6.05 and 4.60 ms in Fig. 7b are identified by their isotope patterns as $[A_3B_1 + Na]^+$, $[A_6B_2 + 2Na]^{2+}$ and $[A_9B_3 + 3Na]^{3+}$, respectively. Although only one sequence is possible for the singly charged components, as mentioned above, the higher charge states can exist in different types of branching depending on the sequence of A and B repeat units. The observation of single peaks for the higher charge states strongly suggests, however, that not all possible sequences are formed and/or that larger, differently branched isomers may be very similar in overall shape (architecture) to be dispersed under our IM-MS conditions. Unfortunately, the absolute ion intensities of the mobility dispersed signals were too low to study their fragmentation characteristics by IM-MS^2 experiments.

IM separation of the $[M + Na]^+$ ion from A_2B_2 (*m/z* 1875) also leads to three signals, peaking at 11.37, 6.68 and 5.05 ms (*cf.* Fig. 7c). The corresponding isotope patterns reveal the compositions $[A_2B_2 + Na]^+$, $[A_4B_4 + 2Na]^{2+}$ and $[A_6B_6 + 3Na]^{3+}$, respectively. Only a single peak is detected for the singly charged A_2B_2. Hence, this stoichiometry results in the formation of mainly one sequence/architecture, or both structures consistent with the MS^2 data coexist but are too similar in shape/size for differentiation by IM-MS. To resolve this issue, the collision cross-section (CCS) of sodiated A_2B_2 was derived from the drift time of this ion in the IM cell

(11.37 ms, Fig. 7c) and compared with theoretical predictions of the CCSs of the two possible candidates, B(B)A_2 and B(A)B(A).

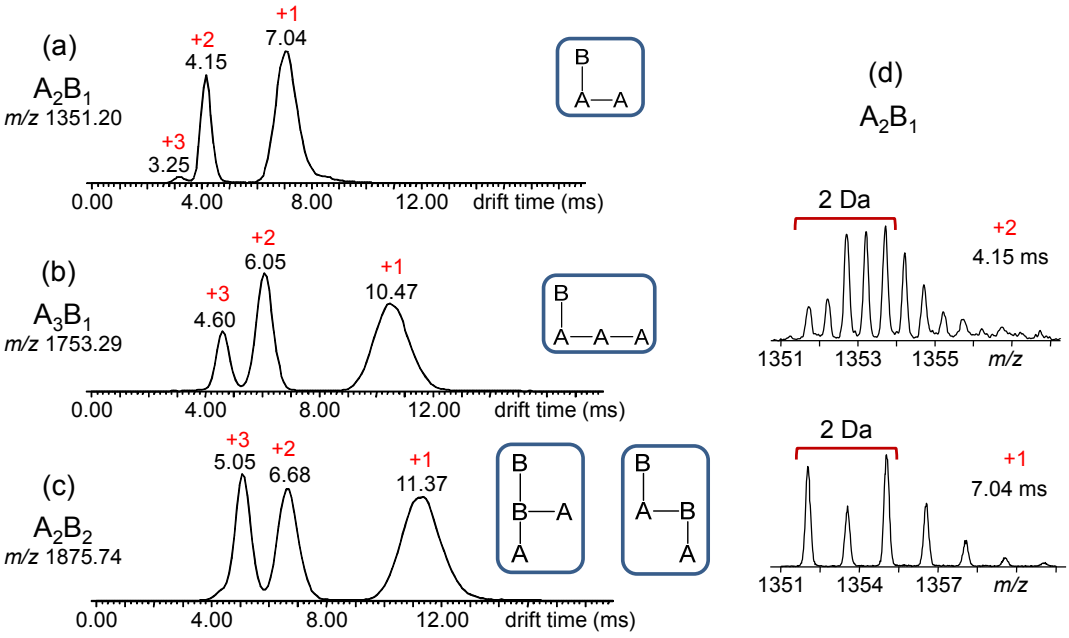

Fig. 7. ESI-IM-MS drift time distributions of sodiated (a) A_2B_1 (*m/z* 1351.3), (b) A_3B_1 (*m/z* 1753.4) and (c) A_2B_2 (*m/z* 1875.3); at each *m/z* value, three peaks are observed, corresponding to ions with +1 to +3 sodium charges. (d) Charge states were determined from the isotope patterns in the mass spectra extracted from each IM-separated peak, as exemplified for the +2 and +1 peaks of A_2B_1.

The ion mobility and, hence, drift time of an ion through the IM region depends on its charge and CCS which is a measure of the ion's size (mass) and shape (architecture).[40-42] With the traveling wave variant of IM-MS utilized in our study, drift times cannot be converted to collision cross-sections through a mathematical equation but require calibration of the drift time scale with standards of known CCS.[60,61] A calibration curve was constructed using peptide and protein ions (Fig. S3),[63] which renders a CCS of 327 Å^2 for A_2B_2 (± <4%).

Molecular modeling was employed to calculate the CCS of $B(B)A_2$ and $B(A)B(A)$. For each isomer, 150 structures were energy-minimized by annealing simulations and their collision cross-sections were calculated by the projection approximation (PA) method. The PA method ignores scattering losses and interactions between the ion and the bath gas in the IM cell, which are included in the more rigorous trajectory method, but nevertheless has been demonstrated to generate CCSs in good agreement with experimental values for relatively small (<2000 Da), quasi spherical structures, such as the ones considered in this study (*cf.* Fig. 6b).[67-69] The resulting CCS *vs.* energy plots (Fig. S4) reveal that all 150 optimized structures of each isomer are grouped closely together in one architectural family. The average calculated collision cross-section of the 150 structures is 338 $Å^2$ for $B(B)A_2$ and 352 $Å^2$ for $B(A)B(A)$. CCS differences of this magnitude can be distinguished with the IM-MS instrumentation used in this study, as was recently shown for *ortho*-, *meta*- and *para*-substituted polyhedral oligomeric silsesquioxane.[54]

It is worth noting that the drift time distributions of $[A_2B_2 + Na]^+$ and $[A_3B + Na]^+$, which have comparable masses, are very similar (*cf.* +1 peaks in Figs. 7b and 7c). Since $[A_3B + Na]^+$ only has one sequence (*vide supra*), this similarity strongly suggests that $[A_2B_2 + Na]^+$ too comprises mainly one sequence; the presence of a significant amount of a second architecture would have resulted in a distorted peak shape with a recognizable shoulder.[51,54]

The experimentally deduced collision cross-section of sodiated A_2B_2, 327 (±13) $Å^2$, agrees reasonably well (within ~3%) with the calculated CCS of the branched architecture $B(B)A_2$, 338 $Å^2$, but is substantially different (by ~8%) from the CCS of the isomeric architecture $B(A)B(A)$, 352 $Å^2$. Thus, the combined MS^2 and IM-MS data provide evidence that the most probable tetrameric sequence of the glycopolymer is the branched structure $B(B)A_2$.

CONCLUSIONS

MALDI mass spectrometry confirmed the successful copolymerization of the monomer (A) and inimer (B) used to prepare a hyperbranched polyacrylate-based glycopolymer with mannose substituents in the acrylate ester pendants and at the branching points. Its molecular weight increased substantially with the number of inimer units incorporated, consistent with simultaneous growth of branches at the inimer sites.

MALDI and ESI combined with MS^2 and MS^n experiments showed that energetically activated $[M + Na]^+$ ions of the glycopolymer, in which all sugar hydroxy groups were acetylated, dissociate mainly *via* charge remote 1,5-H rearrangement fragmentations over either the acetyl protecting groups or the mannose pendant ester groups, leading to losses of acetic acid and dehydrated mannose, respectively. Backbone C–C bond cleavages, which could have revealed information about the sequence of A and B repeat units, were not observed.

The copolymerization method utilized (ATRP), led to a glycopolymer with the composition A_nB_m and *m* Br substituents. All Br atoms remained bound to the polymer during MALDI or ESI analysis. An important finding of this study was that sodiated A_nB_m oligomers underwent elimination of CH_3Br under MS^2 conditions, if they contained an inimer unit (B) attached through its initiating site to a terminal repeat unit. Only with this specific arrangement, a rearrangement took place, causing the elimination of a terminal Br and a CH_3 group from the inimer's $COOCH_3$ substituent. Because of its specificity, this fragmentation provided unique sequence insight on the architecture of A_1B_2 and A_2B_2 oligomers, whose MS^2 characteristics could only be reconciled with the sequence B(B)(A) for the former and the sequences $B(B)A_2$ and/or B(A)B(A) for the latter.

Supplementary information that helped to distinguish between the two mentioned alternative A_2B_2 structures was provided by IM-MS. Dispersion of the sodiated A_2B_2 beam by its ion mobility indicated the presence of only one A_2B_2 component with a collision cross-section of 327 $Å^2$, which matched within experimental error (4%) the CCS predicted theoretically for the $B(B)A_2$ architecture (338 $Å^2$) and was significantly different from the CCS predicted for the isomeric B(A)B(A) architecture (352 $Å^2$). A difference of 14 $Å^2$ in CCS would be sufficient to separate the $B(B)A_2$ and B(A)B(A) isomers or lead to recognizably distorted IM-MS signals under our conditions.[51,54] Hence, the combined tandem MS and ion mobility MS data provided evidence that the preferred tetrameric A_2B_2 architecture has the branched sequence $B(B)A_2$ (see more detailed structures or symbols in Figs. 6 and 7).

The two identified sequences, *viz.* B(B)(A) for the A_1B_2 trimer and $B(B)A_2$ for the A_2B_2 tetramer, provide a hint about the polymerization mechanism. Such architectures would arise if dimer B(A) is formed first and continues to grow by reacting with the acrylate group of a second inimer unit to form B(B)(A) and subsequently with the acrylate group of another monomer to form $B(B)A_2$. Further propagation through such steps creates more branches and ultimately, as more B and A units are copolymerized, a hyperbranched material.

ACKNOWLEDGEMENTS

We thank the National Science Foundation (CHE-1308307 to C.W. and CHE-1112490 to A.M.K.) for financial support and George R. Newkome for the use of the Materials Studio software. K.L. was supported by a fellowship from the NIH Biotechnology Training Program, T32GM067555.

REFERENCES

1. N. Sharon and H. Lis, *Sci. Am.*, 1993, **268**, 82-89.
2. Y. C. Lee and R. T Lee, *Acc. Chem. Res.*, 1995, **28**, 321-327.
3. M. Mammen, S. K. Chio and G. M. Whitesides, *Angew. Chem. Int. Ed.*, 1998, **37**, 2754-2794.
4. R. T. Lee and Y. C. Lee, *Glycoconjugate J.*, 2000, **17**, 543-551.
5. I. Capila and R. J. Linhardt, *Angew. Chem., Int. Ed.*, 2002, **41**, 391-412.
6. C. R. Bertozzi and L. L. Kiessling, *Science*, 2001, **291**, 2357-2364.
7. V. Ladmiral, E. Melia and D. M. Haddleton, *Eur. Polym. J.*, 2004, **40**, 431-449.
8. S. Muthukrishnan, G. Jutz, X. André, H. Mori and A. H. E. Müller, *Macromolecules*, 2005, **38**, 9-18.
9. Y. Wang and K. L. Kiick, *J. Am. Chem. Soc.*, 2005, **127**, 16392-16393.
10. C. R. Becer, *Macromol. Rapid Commun.*, 2012, **33**, 742-752.
11. Y. Miura, *Polym. J.*, 2012, **44**, 679-689.
12. E. Dickinson and B. Bergenstahl (Eds.), *Food colloids: proteins, lipids, and polysaccharides*, The Royal Society of Chemistry: Cambridge, 1997 (vol. **192**).
13. J. K. F. Suh and H. W. T. Matthew, *Biomaterials*, 2000, **21**, 2589-2598.
14. S. H. Kim, M. Goto, C. S. Cho and T. Akaike, *Biotechnol. Lett.*, 2000, **22**, 1049-1057.
15. H. Sashiwa, J. M. Thompson, S. K. Das, Y. Shigemasa, S. Tripathy and R. Roy, *Biomacromolecules*, 2000, **1**, 303-305.
16. S. G. Spain and N. R. Cameron, *Polym. Chem.*, 2011, **2**, 60-68.
17. J. Zaia, *Mass Spectrom. Rev.*, 2004, **23**, 161-227.
18. L. Bindila and J. Peter-Katalinic, *Mass Spectrom. Rev.*, 2009, **28**, 223-253.

19. D. J. Harvey, *Mass Spectrom. Rev.*, 2012, **31**, 183-311.

20. P. Mischnick, *Adv. Polym. Sci.*, 2012, **248**, 105-174.

21. A. El-Hawiet, E. N. Kitova and J. S. Klassen, *Biochemistry*, 2012, **51**, 4244-4253.

22. M. J. Kailemia, L. R. Ruhaak, C. B. Lebrilla and I. J. Amster, *Anal. Chem.*, 2014, **86**, 196-212.

23. V. N. Reinhold, B. B. Reinhold, and C. E. Costello, *Anal. Chem.*, 1995, **67**, 1772-1784.

24. H. J. An and C. B. Lebrilla, *Mass Spectrom. Rev.*, 2011, **30**, 560-578.

25. G. O. Staples and J. Zaia, *Curr. Proteomics*, ***2011***, **8**, 325-336.

26. G. Adamus, W. Sikorska, M. Kowalczuk, I. Noda and M. M. Satkowski, *Rapid Commun. Mass Spectrom.*, 2003, **17**, 2260-2266.

27. A. T. Jackson, J. H. Scrivens, J. P. Williams, E. Shammel Baker, J. Gidden and M. T. Bowers, *Int. J. Mass Spectrom.*, 2004, **238**, 287-297.

28. P. Rizzarelli, C. Puglisi and G. Montaudo, *Rapid Commun. Mass Spectrom.*, 2005, **19**, 2407-2418

29. C. Wesdemiotis, F. Pingitore, M. J. Polce, V. M. Russell, Y. Kim, C. M. Kausch, T. H. Connors, R. E. Medsker and R. R. Thomas, *Macromolecules*, 2006, **39**, 8369-8378.

30. P. Terrier, W. Buchmann, B. Desmazières and J. Tortajada, *Anal. Chem.*, 2006, **78**, 1801-1806.

31. G. Adamus, *Rapid Commun. Mass Spectrom.*, 2007, **21**, 2477-2490.

32. A. P. Gies, M. J. Vergne, R. L. Orndorff and D. M. Hercules, *Macromolecules*, 2007, **40**, 7493-7504.

33. M. J. Polce, M. Ocampo, R. P. Quirk and C. Wesdemiotis, *Anal. Chem.*, 2008, **80**, 347-354.

34. M. J. Polce, M. Ocampo, R. P. Quirk, A. M. Leigh and C. Wesdemiotis, *Anal. Chem.*, 2008, **80**, 355-362.

35. C. Wesdemiotis, N. Solak, M. J. Polce, D. E. Dabney, K. Chaicharoen and B. C. Katzenmeyer, *Mass Spectrom. Rev.*, 2011, **30**, 523-559.

36. V. Scionti and C. Wesdemiotis, In *Mass Spectrometry in Polymer Chemistry*, C. Barner-Kowollik, T. Gründling, J. Falkenhagen and S. Weidner (Eds.), Wiley-VCH: Weinheim, 2012, pp. 57-84.

37. T. Fouquet, C. Chendo, V. Toniazzo, D. Ruch and L. Charles, *Rapid Commun. Mass Spectrom.*, 2013, **27**, 88-96.

38. A. M. Yol, D. E. Dabney, S.-F. Wang, B. A. Laurent, M. D. Foster, R. P. Quirk, S. M. Grayson and C. Wesdemiotis, *J. Am. Soc. Mass Spectrom.*, 2013, **24**, 74-82.

39. A. M. Yol and C. Wesdemiotis, *React. Funct. Polym.*, 2014, **80**, 95-108.

40. M. T. Bowers, P. R. Kemper, G. von Helden and P. A. M. van Koppen, *Science*, 1993, **260**, 1446-1451.

41. D. E. Clemmer and M. F. Jarrold, *J. Mass Spectrom.*, 1997, **32**, 577-592.

42. A. B. Kanu, P. Dwivedi, M. Tam, L. Matz and H. Hill Jr., *J. Mass Spectrom.*, 2008, **43**, 1-22.

43. C. L. Wilkins and S. Trimpin (Eds.), *Ion Mobility Spectrometry-Mass Spectrometry*, CRC Press: Boca Raton, 2011.

44. C. Lapthorn, F. Pullen and B. Z. Chowdhry, *Mass Spectrom. Rev.*, 2013, **32**, 43-71.

45. L. S. Fenn and J. A. McLean, *Meth. Mol. Biol.*, 2013, **951**, 171-194.

46. Y.-T. Chan, X. Li, M. Soler, J. L. Wang, C. Wesdemiotis and G. R. Newkome, *J. Am. Chem. Soc.*, 2009, **131**, 16395-16397.

47. E. R. Broker, S. E. Anderson, B. H. Northrop, P. J. Stang and M. T. Bowers, *J. Am. Chem. Soc.*, 2010, 132, 13486-13494.

48. X. Li, L. Guo, M. Casiano-Maldonado, D. Zhang and C. Wesdemiotis, *Macromolecules*, 2011, **44**, 4555-4564.

49. J. N. Hoskins, S. Trimpin and S. M. Grayson, *Macromolecules*, 2011, **44**, 6915-6918.

50. Y.-T. Chan, X. Li, G. A. Carri, C. N. Moorefield, G. R. Newkome and C. Wesdemiotis, *J. Am. Chem. Soc.*, 2011, **133**, 11967-11976.

51. X. Li, Y.-T. Chan, M. Casiano-Maldonado, J. Yu, G. A. Carri, G. R. Newkome and C. Wesdemiotis, *Anal. Chem.*, 2011, **83**, 6667-6674.

52. V. Scionti, B. C. Katzenmeyer, N. Solak, X. Li and C. Wesdemiotis, *Eur. J. Mass Spectrom.*, 2012, **18**, 113-137.

53. J. R. Snelling, C. A. Scarff and J. H. Scrivens, *Anal. Chem.*, 2012, **84**, 6521-6529.

54. Y. Li, K. Guo, H. Su, X. Li, X. Feng, Z. Wang, W. Zhang, S. Zhu, C. Wesdemiotis, S. Z. D. Cheng and W.-B. Zhang, *Chem. Sci.*, 2014, **5**, 1046-1053.

55. N. Solak Erdem, N. Alawani and C. Wesdemiotis, *Anal. Chim. Acta*, 2014, **808**, 83-93.

56. K. Lin and A. M. Kasko, *Biomacromolecules*, 2013, **14**, 350-357.

57. D. Suckau, A. Reseman, M. Schuerenberg, P. Hufnagel, J. Franzen and A. Holle, *Anal. Bioanal. Chem.* 2003, **376**, 952-965.

58. Bruker Esquire/HCT Series User Manual, version 1.3, Bruker Daltonik GmbH: Bremen, Germany, 2008, **1**, chapter 3.

59. S. D. Pringle, K. Giles, J. L. Wildgoose, J. P. Williams, S. E. Slade, K. Thalassinos, R. H. Bateman, M. T. Bowers and J. H. Scrivens, *Int. J. Mass Spectrom.*, 2007, **261**, 1-12.

60. B. T. Ruotolo, J. Benesch, A. Sandercock, S.-J. Hyung and C. V. Robinson, *Nat. Protoc.* 2008, **3**, 1139-1152.

61. K. Thalassinos, M. Grabenauer, S. E. Slade, G. R. Hilton, M. T. Bowers and J. H. Scrivens, *Anal. Chem.*, 2009, **81**, 248-254.

62. B. C. Katzenmeyer, L.R. Cool, J.P. Williams, K. Craven, J.M. Brown and C. Wesdemiotis, *Int. J. Mass Spectrom.*, 2014, in press (doi: 10.1016/j.ijms.2014.09.021).

63. http://www.indiana.edu/~clemmer/Research/Cross%20Section%20Database/Peptides/polyaminoacid_cs.htm and http://www.indiana.edu/~clemmer/Research/Cross%20Section%20Database/Proteins/protein_cs.htm (accessed on 26 November 2014).

64. M. F. Mesleh, J. M. Hunter, A. A. Shvartsburg, G. C. Schatz and M. F. Jarrold, *J. Phys. Chem.*, 1996, **100**, 16082-16086.

65. K. Chaicharoen, M. J. Polce, A. Singh, C. Pugh and C. Wesdemiotis, *Anal. Bioanal. Chem.*, 2008, **392**, 595-607.

66. P. Mischnick and D. Momcilovic, *Adv. Carbohydr. Chem. Biochem.*, 2010, **64**, 117-210.

67. S. E. Henderson, J. Li, A. E. Counterman and D. E. Clemmer, *J. Phys. Chem. B*, 1999, **103**, 8780-9785.

68. T. W. Knapman, J. T. Berryman, J. Campuzano, S. A. Harris and A. E. Ashcroft, *Int. J. Mass Spectrom.*, 2010, **298**, 17-23.

69. C. Bleiholder, T. Wyttenbach and M. T. Bowers, *Int. J. Mass Spectrom.*, 2011, **308**, 1-10.